Steady and Transient Heat Transfer Characteristics of Flat Micro Heatpipe

*by Yuichi Kimura *, Yoshio Nakamura *, Junji Sotani *2 and Masafumi Katsuta *3*

ABSTRACT Recently, a flat micro heatpipe of slim-profile for use in electronic equipment like personal computers is drawing attention because of its ease of mounting and attachment to heat sources. In this paper steady-state heat transfer characteristics of this heatpipe have been experimentally confirmed in detail, and a prediction method for its maximum heat transfer rate is proposed. Moreover in performance measurement, transient heat transfer characteristics due to step input have also been evaluated since actual operation of the heatpipe itself normally starts from room temperature.

In the steady-state measurement, evaluation was carried out while the temperature of adiabatic section of the heatpipe was maintained at 50°C by adjusting the cooling capacity of a fan, and the amount of working fluid and the lengths of evaporating and condensing sections were taken as parameters. As the result, it has been confirmed that the maximum heat transfer rate increases as the amount of working fluid increases, and that the longer the lengths of evaporating and condensing sections, the greater the maximum heat transfer rate. In view of these results, the equation of pressure balance has been reexamined in order to predict the maximum heat transfer rate more accurately.

In the transient-state measurement, temperature rise due to step input was held constant by adjusting the cooling capacity of Peltier elements mounted on the condensing section of the heatpipe, and the amount of working fluid, the temperature of heatsink and the time interval of step input were taken as parameters. As the result, it has been confirmed that the maximum heat transfer rate measured using a step input becomes smaller than that of the steady state due to the lowered working temperature.

1. INTRODUCTION

In recent years, laptop PCs are proceeding to have diversification of onboard devices and downsizing of the casing, while the heat generation rate of the CPU continues to increase —rather contradicting factors because basically the higher the heat generation rate, the greater the heat-dissipating space needed. Accordingly in the near future, there will be a need for a new cooling technology [1] that can improve design flexibility, needed space and heat-dissipating performance to solve these problems.

Thus micro heatpipes (hereafter called μHP) are beginning to be used as a cooling device for laptop PCs. The category of heatpipes generally include various new heatpipes [2)~6)] that are under extensive and detailed study such as self-exciting mode oscillating-flow (SEMOS) heatpipe, oscillating-flow heatpipe, pulsating heatpipe (PHP) and capillary pumped loop (CPL) heatpipe, and it is expected that these new heat transfer devices will possibly see practical applications.

The slim-profiled flat μHP that has recently been developed is drawing attention because the heatpipe has the advantages of ease of mounting in PCs assuring a sufficient contact surface with heat-generating devices. While this flat μHP has geometrical features such that its cross-sectional area of the vapor channel for the working fluid is very small in comparison with cylindrical heatpipes, the effects of this feature on the working principle and the heat transfer performance have not been clarified yet. Accordingly, this paper presents the basic data of this flat μHP together with thermal characteristics that are indispensable for optimizing its inner structure.

2. EXPERIMENTAL SETUP AND METHOD

Figure 1 shows the experimental setup for thermal performance measurement consisting of the main test apparatus, a power supply and a data acquisition system combined with a personal computer. As shown in Figure 2, the μHP sample was provided with a micro ceramic

* Ecology and Energy Lab., R&D Div.
*2 Electronics and Automotive Systems Co.
*3 Advanced Research Institute for Science and Engineering, Waseda Univ.

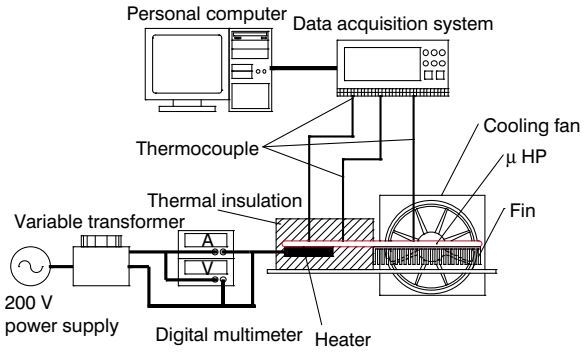

Figure 1 Schematic of experimental setup.

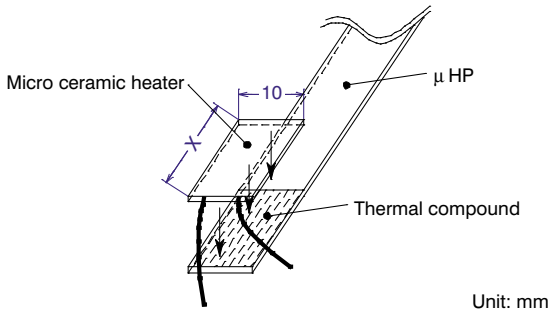

Figure 2 Detail of heater and evaporating section.

Table 1 Sample and conditions for evaluation.

Length of HP (mm)	157
Thickness of HP (mm)	1.0
Length of evaporating section (mm)	10, 20, 30, 40, 50
Length of condensing section (mm)	40, 60, 80, 100
Amount of working fluid (vol%)	20, 25, 30, 35, 40, 45

heater for heat input, whose length —marked by X in the Figure— could be changed to make it adapted to various test conditions. To enhance thermal conduction from the heater to the μHP sample, thermal compound was applied to the interface, and the evaporating and adiabatic sections were thermally insulated using a thermal insulation so that all the input heat was dissipated through the condensing section. At the condensing section, a fin array with a fan was used for sufficient cooling, while the capacity of the fan was adjusted to maintain a constant temperature of 50°C in the adiabatic section. All the experiments for steady-state measurement were carried out under the condition of 50°C for the adiabatic section, and besides, all the data were taken after the temperature of this section was stabilized.

With respect to the μHP sample, braided wire of copper was used as wick; deionized water was used as working fluid; the length and the thickness of all the samples were 157 mm and 1 mm, respectively, as shown in Table 1; and K-type thermocouples were mounted on the surface at an interval of 5 mm totaling 29 in number.

The experiments were carried out, taking the amount of working fluid and the lengths of evaporating and condensing sections as parameters, with the aim of clarifying the thermal characteristics of flat μHPs as well as of proposing a capillary force-based prediction method for the maximum heat transfer rate that is useful for many applications.

2.1 Heat Transfer Coefficient and Maximum Heat Transfer Rate

The heat transfer coefficient h_e was calculated by the The heat transfer coefficient h_e was calculated by the equation

$$h_e = \frac{Q}{A(T - T_{ad})} \tag{1}$$

Figure 3 shows the relationship between the heat transfer coefficient at the evaporating section and heat input.

In the Figure, dryout occurs at a point where the heat transfer coefficient shows a marked drop, and the maximum heat transfer rate is defined as the heat input at the point just before dryout. Accordingly, as can be seen from

Nomenclature

a	half width of vapor channel
A	surface area
b	half height of vapor channel
d	diameter of screen wire
D_ℓ	hydraulic diameter
$fRe_{D\ell}$	Poiseuille number
g	gravitational constant
h	heat transfer coefficient
H_{fg}	latent heat of evaporation
H_ℓ	height of liquid channel
K	permeability
L	length of heatpipe
N	pore number
P	pressure
Q	input heat
R	gas constant
r_c	effective pore radius
r_r	effective pore radius
s	aspect ratio
S	surface area
T	temperature
$\overline{u}_\ell$	mean velocity
V^+	amount of working fluid

Greek letters

ΔP	pressure loss, or pressure driving force
α	coefficient of evaporation and condensation
ε	void ratio
ζ	shrinkage factor
θ	contact angle
μ	viscosity
ρ	density
σ	surface tension
τ	shearing stress
ϕ	contact angle
Ψ	non-dimensional pressure drop

Subscripts

ad	adiabatic
c	capillary force
con	condensation
e	evaporation
eff	effective
eva	evaporation
g	gas
ℓ	liquid, or liquid flow
lc	liquid channel
s	slag, or paddle
v	vapor
v'	vapor
vc	vapor channel
w	wick

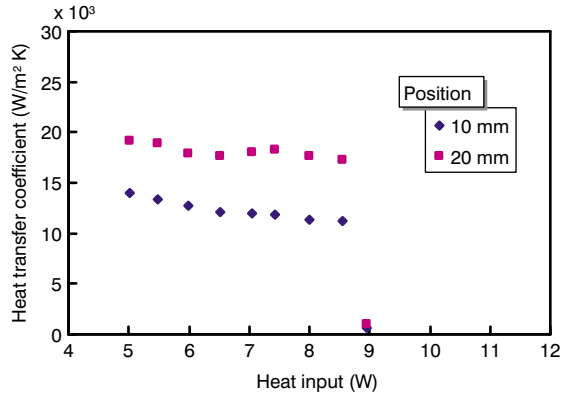

Figure 3 Relationship between the heat transfer coefficient and heat input.

Figure 3, the valued of 8.5 W was taken as the maximum heat transfer rate for this μHP.

3. EXPERIMENTAL RESULTS AND DISCUSSIONS

3.1 Steady-State Measurement

3.1.1. Redefinition of Effective Length

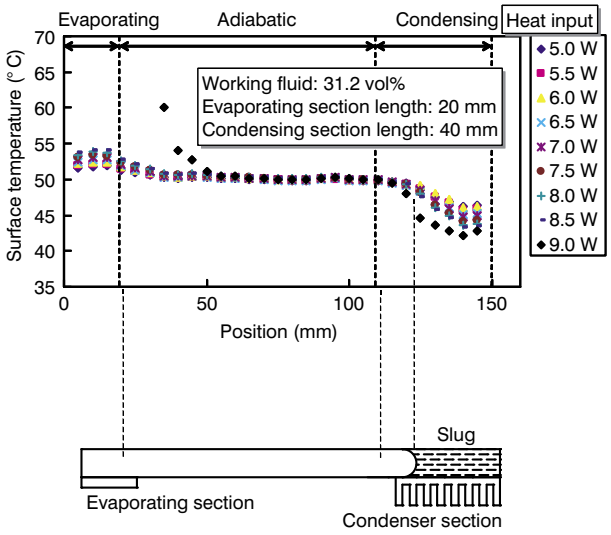

Figure 4 Temperature distribution on μHP.

Figure 4 shows a temperature distribution on the surface of a μHP. A marked temperature drop is observed at the end of the condensing section, presumably caused by a liquid slug. Thus it is thought that the effective length of a μHP L_{eff} representing the circulation length of working fluid has to be redefined as different from the conventional, taking the length of the liquid slug into consideration as follows.

$$L_{\mathrm{eff}}=\frac{L_{\mathrm{e}}}{2}+L_{\mathrm{ad}}+\frac{L_{\mathrm{c}}-L_{\mathrm{s}}}{2} \tag{2}$$

$$L_{\mathrm{s}}=\frac{V^{+}-S_{\ell\mathrm{c}}\times L/\zeta}{S_{\mathrm{vc}}} \tag{3}$$

When a μHP is placed horizontally, and if the capillary force associated with the size of the vapor channel is greater than the difference in the gravitational force due to a different channel height, the surplus fluid turns into a liquid slug at the end of the condensing section without being dispersed over the pipe length. The condition for liquid slug formation can be represented by the following equation.

$$\frac{2\sigma}{r_{\mathrm{r}}}\cos\phi>\rho_{\ell}\times g\times H_{\ell} \tag{4}$$

3.1.2. Heat Transfer Performance

Figure 5 shows the relationship between the maximum heat transfer rate and the length of condensing section of μHP with braided wire wick having different amounts of working fluid, using the length of evaporating section as a parameter. It can be seen from the Figure that the maximum heat transfer rate increases as the length of either the evaporating section or the condensing section increases. In view of the capillary force, this is attributable to the fact that, in either case mentioned above, the length of the adiabatic section shortens resulting in shortening of the effective length, in addition to reduction of the pressure loss. When the lengths of the evaporating and condensing sections are equal, it is seen that the maximum heat transfer rate increases as the amount of working fluid increases. It is suggested that the more the encapsulated working fluid the more surplus it becomes, so that the fluid forms a liquid slug at the condensing section end thereby bringing an effect equivalent to shortening of the effective length of the μHP. Consequently, it is assumed that the surplus amount forms a liquid slug as shown in Figure 4.

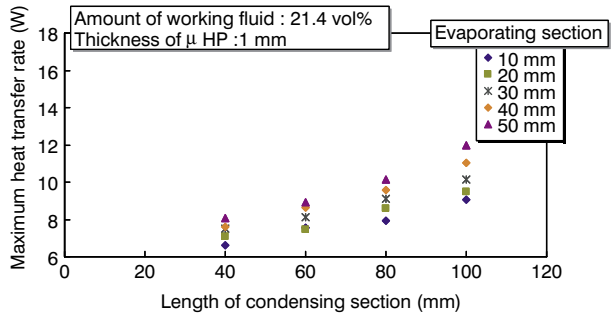

a) Amount of working fluid: 21.4 vol%

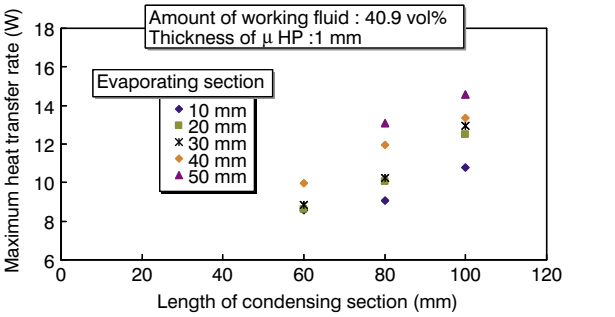

b) Amount of working fluid: 40.9 vol%

Figure 5 Maximum heat transfer rate of μHPs with different amount of working fluid.

3.1.3. Prediction Equation for Maximum Heat Transfer Rate

Judging from the experiments above mentioned, it is suggested that the conventional model for heatpipes, i.e. capillary force-based model, applies to this flat μHP also. Accordingly, the following model for the braided wire wick was used to predict the maximum heat transfer rate.

Figure 6 shows a flat μHP model with an ideal braided wire wick, whereby the wick is assumed to be located at the center of the pipe, and liquid channels are formed in the space between the wires as shown in the enlarged illustration in the Figure. Table 2 shows the dimensions of the wick configuration.

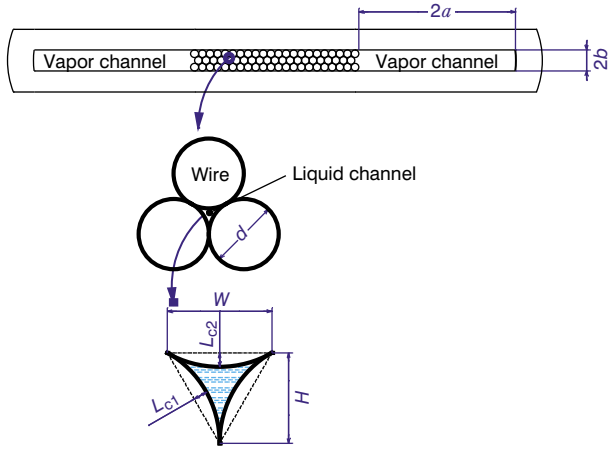

Figure 6 Cross-section of flat μHP and enlarged illustration of wick.

Table 2 Dimensions of the wick configuration shown in Figure 6.

a	1.938 mm
b	0.250 mm
d	0.104 mm
W	0.052 mm
H	0.052 mm
L_{c1}	0.00697 mm
L_{c2}	0.00697 mm

Important parameters of permeability K [4] and effective pore radius r_c [5] are given by the following equations.

$$K=\frac{D_\ell{}^2\times N}{2\times fRe_{D\ell}} \tag{5}$$

$$r_c=\frac{d+\sqrt{32\times K/\varepsilon}}{2} \tag{6}$$

Another important parameter of Poiseille number $fRe_{D\ell}$ can be uniquely determined from the geometrical configuration of the cross-section. Pressure balance is taken into consideration to predict the maximum heat transfer rate, that is, a pressure drop is generated by the working fluid in circulation, and normal circulation of the working fluid is interrupted when the driving force due to capillary force can no longer overcome the pressure drop, reaching a limit of heat transfer whose condition can be represented by:

$$\Delta P_c-\Delta P_s\geq\Delta P_v+\Delta P_\ell+\Delta P_{eva}+\Delta P_{con} \tag{7}$$

Each term in Equation (7) is explained in the following.

(1) Driving force due to capillary force: ΔP_c

The capillary force of the wick acts as a driving force for normal circulation of the working fluid [9], and is represented by:circulation circulation circulation

$$\Delta P_c=\frac{2\sigma}{r_c}\cos\theta \tag{8}$$

While the contact angle θ for a combination of copper and water is said to range generally between 33°～ 40°, a value of 38° was adopted because this is most frequently used [4].

(2) Pressure drop due to liquid flow: ΔP_ℓ [3]

According to Darcy's Law, ΔP_ℓ can be represented by using the above-mentioned K value as follows.

$$\Delta P_\ell=\frac{\mu_\ell Q}{KA_w\rho H_{fg}}L_{eff} \tag{9}$$

(3) Pressure drop due to evaporation and condensation: ΔP_{eva} and ΔP_{con} [10), 11)]

These can be calculated from an analysis based on molecular dynamics using the following equations.

$$\Delta P_{eva}=\sqrt{\frac{RT}{2\pi}}\times\frac{Q}{\alpha(H_{fg}-(1/2)RT)A_{eva}} \tag{10}$$

$$\Delta P_{con}=\sqrt{\frac{RT}{2\pi}}\times\frac{Q}{\alpha(H_{fg}-(1/2)RT)A_{con}} \tag{11}$$

(4) Pressure drop due to liquid slug: ΔP_s [7]

When a liquid slug is formed, not only that portion does not function as a heatpipe, but also a pressure drop occurs due to its existence. As shown in Figure 7, a pressure difference in capillary force appears due to the slug formation at the pipe end, lowering the air-liquid interface pressure P_g over the vapor pressure P_v [7].

$$\Delta P_s=P_v-P_g=\frac{2\sigma}{r_r}\cos\theta \tag{12}$$

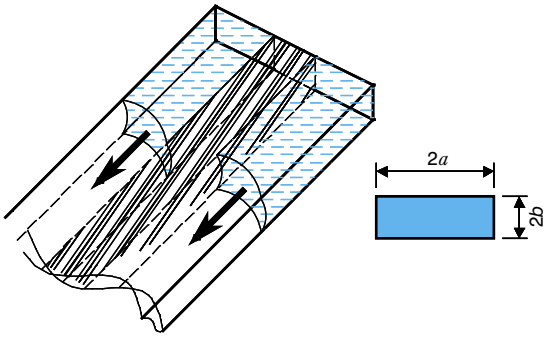

Figure 7 Configuration of liquid slug.

Effective pore radius r_r corresponding to the vapor space can be represented by Equation (13).

$$r_r = \frac{2ab}{a+b} \tag{13}$$

(5) Pressure drop due to vapor flow: P_v

Although the pressure drop due to vapor flow has heretofore been calculated by a simplified equation for pressure drops for a circular cross-section using an equivalent radius, the equation is considered to be insufficient for the calculation of flat μHPs with an extremely small ratio of b/a. Therefore, analysis of rectangular cross-section flow [9] has been carried out to obtain a more accurate expression for the pressure drop due to vapor flow. As illustrated in Figure 8, the pressure drop in one of the vapor channels is calculated based on a rectangular cross-section model as follows.

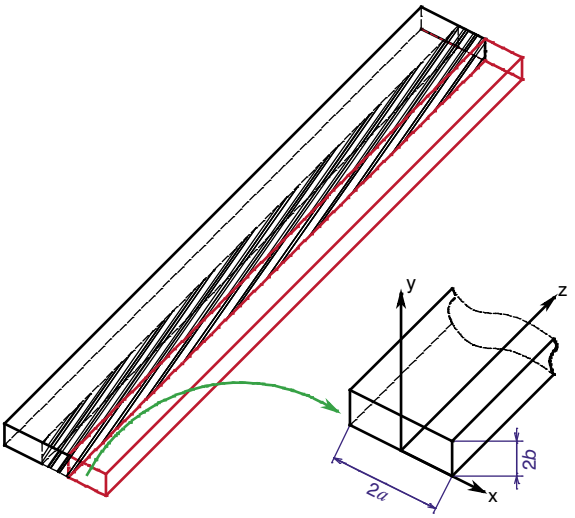

Figure 8 Configuration of vapor channel with rectangular cross-section model.

$$\Delta P_v = \frac{12\mu Q}{\rho a d D^2 H_{fg}(1+s)^2\left(1-48\,s\times 4\tanh\frac{\pi}{2s}\right)} L_{eff} \tag{14}$$

Using Equations (5) through (14), the maximum heat transfer rate can be calculated to obtain a predictive value. It was found that, when the experimental and calculated results were compared, generally speaking the calculated value was higher than the experimental value. As a cause for this, it may be that the actual heat transfer process involves an additional factor of vapor-liquid interaction, and accordingly, investigation was carried out concerning this factor.

(6) Vapor-liquid interaction

In view of the study by Kyu Hyung Do et al. [4], it is thought that there is an interaction between the countercurrents of vapor and liquid even in the case of the braided wire wick, although the interaction may be less significant than in the case of a groove wick having a large contact surface between the two phases of vapor and liquid. Considering that this interaction influences the characteristics of flat μHP as well, the following equations proposed by the aforementioned authors were applied to the μHP, where Ψ denotes non-dimensional pressure drop [3].

$$\Delta P_v' = (1+\psi)\Delta P_v \tag{15}$$

$$\psi = \frac{2b\tau_v}{\mu \bar{u}_\ell} \tag{16}$$

The equation is used in an iterative manner in which the maximum heat transfer rate is calculated first without considering the pressure drop due to vapor-liquid interaction, and subsequently, the rate is recalculated in turn taking the pressure drop into consideration using the first result. Figure 9 shows the iteratively calculated results, where the maximum heat transfer rates are compared between the predicted values based on Equation (7) and the experimental values that change, under the influence of the lengths of condensing and evaporating sections, according to the amount of working fluid.

As can be seen from the Figure, the experimental and predicted values show good agreement, confirming the validity of Equation (7), which aimed at predicting the maximum heat transfer rate analytically based on the concept of pressure balance due to capillary force. In case the amount of working fluid is changed, prediction can be made accurately by introducing a suitable effective length into the Equation.

Thus it has become clear that the pressure drop due to vapor flow near dryout accounts for a large portion of the total pressure drop.

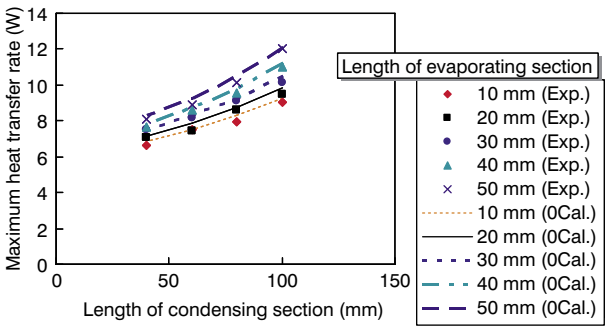

a) Amount of working fluid: 21.4 vol%

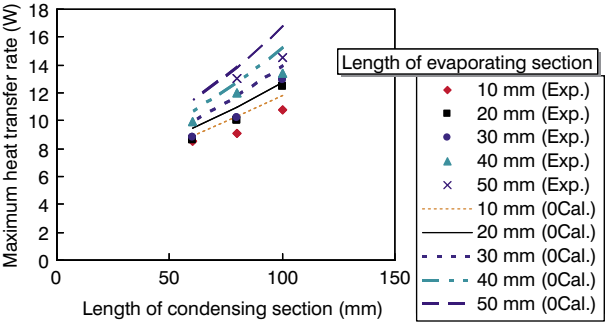

b) Amount of working fluid: 40.9 vol%

Figure 9 Comparison of maximum heat transfer rate between calculated and experimental values.

3.2 Transient-State Measurement

The conditions for the transient-state measurement were such that temperature rise due to step input was held constant by adjusting the cooling capacity of Peltier elements mounted on the condensing section; the amount of working fluid, heatsink temperature and time interval of step input were taken as experimental parameters; transient data were measured from just before the heat input to the steady state; and the transient-state experiments were repeated until dryout. Figure 10 shows the temperature changes of selected sections in response to step input, and Table 3 compares the maximum heat transfer rates of the steady- and transient-state measurements in conjunction with different amounts of working fluid.

It can be seen that, although rather dependent on the working temperature, the maximum heat transfer rate for the transient state is generally lower than that for the steady state, and the rate becomes lower as the cooling temperature decreases. Consequently, in practical applications for cooling IC chips and the like, it is necessary for the design to have a margin of 20 % to 30 % with respect to the heat rate to be dissipated.

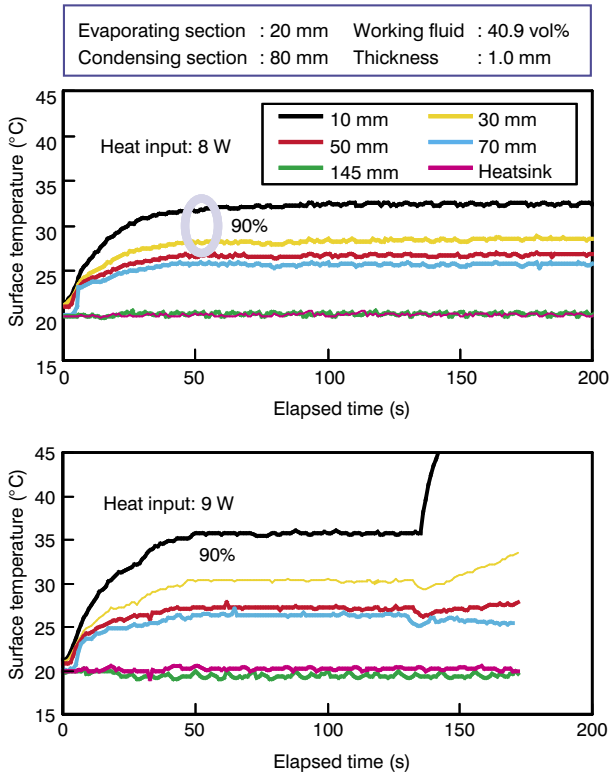

Figure 10 Maximum heat transfer rates under steady- and transient-state conditions.

Table 3 Comparisons of maximum heat transfer rates under steady- and transient-state conditions.

Amount of working fluid (vol%)	Steady state	Transient state	
	Adiabatic section temp.: 50°C	Cooling temp.: 20°C	Cooling temp.: 10°C
20.4	8.09 W	6.01 W	4.97 W
31.2	8.51 W	7.03 W	6.04 W
40.9	10.05 W	9.01 W	8.05 W

Length of evaporating section: 20 mm
Length of condensing section: 80 mm

4. CONCLUSION

(1) With respect to a flat μHP with braided wire wick, the effective length has been redefined, and a pressure-balance equation based on capillary force has been proposed enabling the prediction of maximum heat transfer rate.

(2) Using a prediction equation for maximum heat transfer rate, it has been shown that the pressure drop due to vapor flow accounts for a dominant portion of the total pressure drop.

(3) It has been confirmed that the maximum heat transfer rate for the transient state is lower than that for the steady state, and the rate becomes lower as the cooling temperature decreases.

REFERENCES

1) J. Niekawa et al.: "Introduction to Micro-Heatpipe and Heat Dissipation Technology," Nikkan Kogyo Shimbun Publishing, (1999). (in Japanese)
2) Amir Fagri: HEAT PIPE SCIENCE AND TECHNOLOGY, (1978), Taylor & Francis.
3) Joung Ki Seo: "A Generalized Mathematical Model to Account for the Effect of Liquid-Vapor Interfacial Shear Stress of a Heat Pipe with a Grooved Wick Structure, "The 7th International Heat Pipe Symposium, Jeju, Korea, (2003) 92-96.
4) Kyu Hyung Do: "Mathematical Modeling and Thermal Optimization of a Micro Heat Pipe with Curved Triangular Grooves," The 7th International Heat Pipe Symposium, Jeju, Korea, (2003) 325-331.
5) Hidehiko Noda: "Effect of Mesh Shape on Maximum Capillary Pressure of Plain Weave Screen," The 11th International Heat Pipe Conference, Tokyo, vol 2 (1999) 85-89.
6) H. Kosai et al.: "Heat Transfer Characteristics of a Heatpipe with Composite Metal Screen Wick," Proc. 36th Japan Heat Transfer Symposium, (1999) 653. (in Japanese)
7) M. Murakami et al.: "Heat Transfer Limit of Flat Heatpipe," Trans. JSME, B54-501 (1988) 1157. (in Japanese)
8) H. Kosai et al.: "Effective Pore Radius of Metal Screen Wick," Trans. JSME, B56-521 (1990) 168. (in Japanese)
9) K. Watanabe: "Hydrodynamics —Flow and Loss—," Maruzen Publishing, (2002). (in Japanese)
10) Japan Association for Heatpipe: "Practical Heatpipe," Nikkan Kogyo Shimbun Publishing, (2001). (in Japanese)
11) K. Oshima et al.: "Heatpipe Engineering," Asakura Shoten Publishing, (1981). (in Japanese)